JACS
JOURNAL OF THE AMERICAN CHEMICAL SOCIETY

Communication

pubs.acs.org/JACS

Generation, Characterization, and Application of Hierarchically Structured Self-Assembly Induced by the Combined Effect of Self-Emulsification and Phase Separation

Xiuyu Wang, Yi Hou, Li Yao,* Mingyuan Gao,* and Maofa Ge

Beijing National Laboratory for Molecular Science, Institute of Chemistry, Chinese Academy of Sciences, Beijing 100190, China

Supporting Information

ABSTRACT: Hierarchically structured magnetic single-hole hollow spheres (MSHS) have been successfully obtained via a facile self-assembly strategy. This methodology allows the double emulsions generated via the combined effect of self-emulsification and phase separation to provide confinement for directing the self-assembly of magnetic nanoparticles (MNPs). The resulting MSHS fully capitalize on both the multifunctional properties of MNPs and container features of single-hole hollow spheres. Moreover, the magnetic properties showed obvious improvement and can be tuned by modulating the assembled structure. Thus, MSHS can be used as a smart platform with multiple functionalities including image contrast enhancement, selective encapsulation for biomacromolecules, on-demand release, and magnetically guided transport. This strategy is very promising in the design of hierarchically structured assemblies for desired applications in biomedicine and other fields.

Diversified micro/nanolevel hollow spheres have been developed through chemical synthetic routes for various applications in energy storage, catalysis, chemical sensors, and biomedicine.[1] In particular, many interesting phenomena, such as highly effective diffusivity, up-taking capacity for big guest molecules, and selective and controllable encapsulation, have been observed in a new type of single-hole hollow spheres due to the unique structural features compared to their closed-shell counterparts.[2] However, the single-hole hollow spheres previously reported are often made of polymers and silica.[3] Compositionally, when such inert materials become replaced or accompanied by functional materials, multifunctional single-hole hollow spheres can be synthesized, which have the potential to upgrade the current container performance.[4]

Magnetic nanoparticles (MNPs) exhibit promising multifunctional properties that are capable of contrast enhancement in magnetic resonance imaging (MRI), acting as drug carriers, heat generation, and guidance under remote fields.[5] Furthermore, the intrinsic properties of nanoparticles can be improved by coupling and synergic effects through self-assembly into hierarchical structures based on confinement, which has been considered to be a feasible route to obtain novel functional materials.[6] Such assemblies, in turn, would be programmable for their ultimate performance in specific applications. However, organizing MNPs into complex architectures is challenging and unpredictable because the stabilization of such self-assemblies results from a delicate competition among many forces, including van der Waals, Zeeman coupling, magnetic, entropic, hydrophobic force, and other types of particle interactions.[7] The magnitudes and ranges of these forces are complex, which enriches but also complicates the self-assembly process. Currently the assemblies of MNPs with simple structures including linear assemblies,[8] spherical clusters,[9] and worm-like superstructures[10] are being developed to improve MRI contrast. However, organizing MNPs into hollow nanospheres with a single hole is quite limited.

Herein, we developed a facile self-assembly strategy based on double emulsions to design hierarchically structured magnetic single-hole hollow spheres featured with uniform size, controllable hole, and tunable magnetic properties. The obtained MSHS, with functionalities offered by both the magnetic nanomaterial and container features of hierarchical structure, could serve as a smart platform with multifunction including selective loading, precise transport, on-demand release, and real-time location reporting.

In our strategy, MNPs serve as the building blocks, while a double emulsion provides confinement for directing the self-assembly of MNPs. The strategy involved the following three steps to synthesize MSHS: single droplets, double emulsions, and self-assembly (Figure 1a). In the first step, monodisperse single droplets containing dichloromethane, oleic acid-coated Fe_3O_4 nanoparticles (OA-coated Fe_3O_4, Figure S1) and polyethylene glycol (PEG) were generated through a microfluidic device. As displayed in Figure 1b, the dispersed phase flow passes through the exit orifice and subsequently ruptures to form uniform droplets just inside the orifice as a result of hydrodynamic instabilities. Then, the droplets were collected and kept under a saturated dichloromethane vapor atmosphere at a relatively low temperature (2 °C). Interestingly, double emulsions formed after 40 min. To visualize the transformation of a single droplet into the double emulsion (Figure 1c–e), an oil-soluble green fluorescent dye (fluorescein) was added into the dispersed phase. The sequential fluorescent images showed that the diffusive water accumulates and emerges into reversed tiny droplets, resulting in the self-emulsification process.[11] Such tiny water droplets further trigger phase separation and coalesce to form a large single droplet, finally segregating from the organic phase due to a temperature-assisted phase separation.[12] The droplet size increased from 6 to 10 μm. Hence, based on

Received: November 19, 2015
Published: February 2, 2016

DOI: 10.1021/jacs.5b12149
J. Am. Chem. Soc. 2016, 138, 2090–2093

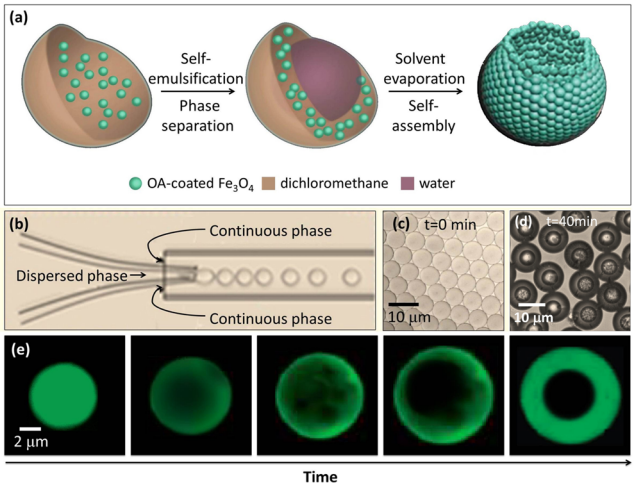

Figure 1. (a) Schematic illustration of the self-assembly strategy based on the double emulsions to produce MSHS. (b) Formation of oil-in-water droplets using a microfluidic device. The dispersed phase consists of MNPs and PEG in dichloromethane, and the continuous phase is the aqueous phase of sodium dodecyl sulfate solution. (c, d) Optical micrographs of single droplets and double emulsions. (e) Sequential fluorescence images showing the transformation of a single droplet into a double emulsion based on the combined effect of self-emulsification and phase separation. A green fluorescent dye was added in the dispersed phase to visually trace the evolution of a single droplet.

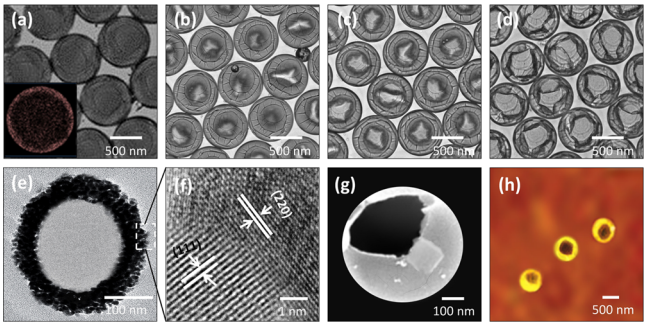

Figure 2. (a–d) TEM images of MSHS produced from emulsion droplets with different C_{PEG}: 0.35, 0.5, 1.0, and 1.5 mg/mL, respectively. Inset: elemental mappings of Fe on intact hollow spheres. (e–h) Typical XTEM, HRTEM, SEM, and AFM images of MSHS-400.

the combined effect of self-emulsification and phase separation, double emulsions were generated without the use of a complex microfluidic device or multiple emulsification steps.[13]

After the formation of double emulsions, dichloromethane was allowed to evaporate slowly into the surrounding air, inducing MNPs to self-assemble in the shell confinement. Upon solvent removal, MNPs tend to aggregate in the shell due to the interparticle interactions including hydrophobic forces, van der Waals forces, and magnetic dipole–dipole interactions.[10] Meanwhile, the decrease in the area of the interface of the shrinking droplets causes a nonequilibrium adsorbed interfacial excess of PEG. As interfacial excess increases, the interfacial energy is predicted to increase to a certain value triggering an interfacial instability (eq 1):[14]

$$d\gamma = \sum_i \nu_i \mu_i \tag{1}$$

where γ is the interfacial free energy, ν_i is the interfacial excess of component i in molecules per unit area, and μ_i is the chemical potential of component i on a per molecule basis. Thus, with the increase of PEG concentration, the shell structures became unstable, which was insufficient to withstand the interfacial energy. Furthermore, the MNPs can produce an uneven distribution of interfacial tension independently (Figure S2), driven by their quasi-irreversible adsorption to the interface of droplets.[15] Consequently, the most unstable part of the shell burst into the continuous phase, resulting in the formation of a single hole. After the release of interfacial energy, the structure of MSHS was stabilized. Therefore, in our experiments, when the initial C_{PEG} was lower than 0.35 mg/mL, monodisperse hollow spheres with closed shells were obtained (Figure 2a). As C_{PEG} increased from 0.5 to 1.5 mg/mL, the diameter of the hole can be tuned by simply adjusting C_{PEG}. When C_{PEG} was above 2.0 mg/mL, extreme instabilities were observed, and the emulsion drops disappeared quickly into the continuous phase.

The structural and morphological characteristics of MSHS were carefully investigated. Transmission electron microscopy (TEM) images (Figure 2b–d) clearly show a series of MSHS. The overall size is ~650 nm, and the diameter of the holes ranges from 150 to 400 nm. We denoted them as MSHS-150, 300, and 400 corresponding to their average hole size, respectively. It is important to highlight that the monodispersity of MSHS is good enough to produce nearly perfect colloidal crystals, which provides a benchmark for the size uniformity of assemblies.[16] Although some narrow crevices occur in the shells, the stability of MSHS has not been destroyed, even under intense vibration, ultrasonic treatment, or magnetic stimuli. Such stability generally originates from the structural features of the shell walls, which are composed of compactly packed nanoparticles and have a uniform thickness (Figures 2e, S3, and S4). Small-angle X-ray scattering (SAXS) measurements indicate the high ordering of the shell structure (Figure S5), where the smaller the hole size, the higher the order of the self-assemble structures is. High-resolution TEM (HRTEM) image of the shell edge (Figure 2f) exhibits the lattice fringes consistent with the interplanar distance of lattice planes of Fe_3O_4 nanoparticles.[17] The morphological features of MSHS were further confirmed by the scanning electron microscope (SEM) and atomic force microscope (AFM) images (Figure 2g,h). Additionally, with the help of PEG, the assembled MSHS possess a high aqueous dispersity, which is demonstrated by dynamic light scattering measurements (Figure S6).

When MNPs are utilized as building blocks to engineer assemblies, the assembled structure becomes an important parameter for determining the magnetic properties besides the composition, crystallographic structure, size, and shape.[18] Here, the ratio of hole size to overall size was used to describe the imperfection of the assembled structures (I_m is 0.231, 0.462, 0.615, and ∞ for MSHS-150, 300, 400, and OA-Fe_3O_4). As shown in Figure 3a, the field-dependent magnetism of MSHS exhibited no hysteresis at 300 K, indicating their superparamagnetic characteristics. The saturation magnetization (M_S) values were determined to be 76.7, 65.2, and 60.5 emu/g for MSHS-150, 300, and 400, respectively, which were nearly twice as high as that of the individual Fe_3O_4 nanoparticles. Interestingly, the decrease of I_m can lead to a systematic increase of M_S of MSHS (Figure 3b). It may be ascribed to the fact that magnetic dipole–dipole interactions between MNPs, also called dipolar coupling, in a relatively

DOI: 10.1021/jacs.5b12149
J. Am. Chem. Soc. 2016, 138, 2090–2093

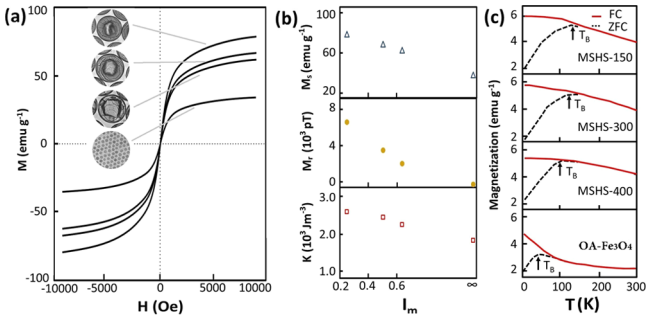

Figure 3. Magnetic properties of MSHS and individual OA-Fe_3O_4 nanoparticles. (a) $M-H$ curves at 300 K. (b) Structural imperfection dependence of M_S, M_r, and K. (c) FC/ZFC magnetization curves.

perfect assembly are much stronger than those of individual nanoparticles or random aggregation patterns.[9] Such stronger coupling interactions within MSHS can be further confirmed by remanence measurements (M_r).[19] The individual Fe_3O_4 nanoparticles showed no remanence. However, M_r of MSHS was obviously enhanced and increased following the decrease of I_m (Figure 3b). Meanwhile, observed from field cooled/zero-field cooled (FC/ZFC) magnetization curves, the blocking temperature T_B of MSHS was shifted to a higher value because the coupling effects in assembled structures suppress thermal fluctuations of magnetic spins.[9] Moreover, the magnetic anisotropy constant K deduced from T_B[20] also increases as I_m decreases (Figure 3b), indicating that by using easily synthesized isotropic building blocks, complex anisotropy in a nanoscale assembly could be created. These results demonstrate that this is a good alternative way to tune the magnetic properties by modulating the assembled structure, making them programmable for the desired performance in specific applications.

To illustrate the applications, the T_2-weighted MRI was performed for the individual nanoparticles and MSHS aqueous solutions at different iron concentrations. Both Fe_3O_4 nanoparticles and MSHS exhibited enhancement in T_2-weighted MRI, where the higher the concentration, the darker the image was. However, MSHS possess a much stronger contrast effect (Figure 4a). To further quantify the results, the transverse relaxation rates (r_2) were determined.[21] MSHS showed remarkably higher values (56, 662, 681, and 694 mM^{-1} s^{-1} for individual nanoparticles, MSHS-150, 300, and 400; Figure S7). They are more than 6-fold of the commercially used Feridex.[22] In general, the r_2 relaxivity increases with M_S due to the magnetic dipole coupling. However, quite unexpectedly, MSHS-400 without the highest M_S showed the strongest T_2 effect among the three different assemblies. It is well-known that MRI is based on the magnetic relaxivity rates of surrounding water molecules. The water accessibility of contrast agents is another essential factor that affects the MR imaging.[23] The higher T_2 effect of MSHS-400 may originate from the synergistic effect of larger hole and higher surface hydrophilicity (Figure S8) that is relevant to the water accessibility.

Compared with the conventional hollow spheres with closed shells, MSHS with controllable single hole and tunable magnetic properties can serve as a supercontainer for the controlled release of big guests or other chemical agents. We used albumin from bovine serum (BSA) as a model biomacromolecule to evaluate the potentials of MSHS for drug delivery. After the loading of BSA, the holes were capped

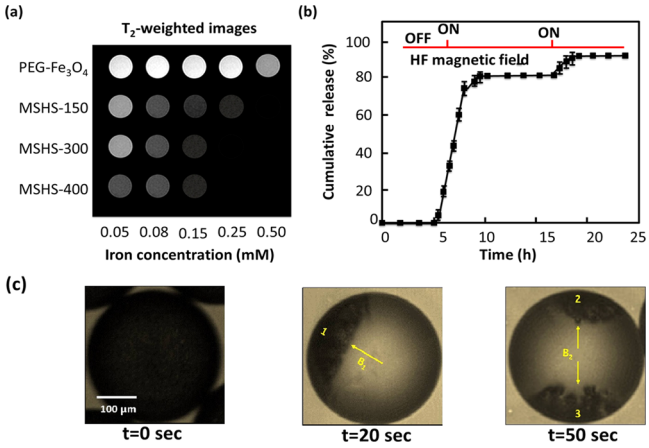

Figure 4. (a) MRI images of MSHS and individual Fe_3O_4 nanoparticles with different concentrations in water. (b) On-demand release profiles of protein from MSHS under the stimuli of 5 min of a HF magnetic field. (c) Magnetically guided transport of MSHS in a droplet. The dark portion is attributed to the MSHS dispersed in the aqueous droplet. The yellow arrows indicate the directions of the applied DC magnetic field.

with a heat-sensitive phase change material (PCM, lauric acid, see Figure S9). When the temperature rises beyond its melting point (43 °C), the PCM can reopen the holes allowing the BSA to diffuse out.[24] Figure 4b shows the on-demand release profile of BSA from MSHS. At 25 °C BSA was not released over 5 h, indicating a perfect sealing by PCM. When 5 min of a high-frequency (HF) magnetic field was applied as a remote-controlled stimuli, MSHS generated heating through Néel and Brownian relaxations.[25] As a result, the encapsulated BSA was instantly released through the reopened holes. When the release reached a balanced status after 12 h, another magnetic stimuli of 5 min triggered a secondary release of residual BSA. The total amount of BSA released reached ~90%. In addition, the uniformity of hollow cavities would enable this drug release system to inject a precise dose of drug, leading to a high reproducibility of drug delivery. Thus, the on-demand drug delivery system can be best fulfilled, which may significantly improve the therapeutic effect and effectively reduce systemic toxicity. Further research will investigate the temperature distribution during heating, thermo tolerance, cytotoxicity, and in vivo distribution of drug containers.

Moreover, magnetically guided transport is another important issue for practical delivery system. However, experimental failure is quite common, mainly due to the absence of good monodispersity and strong magnetism.[26] But our MSHS meet these requirements. The navigation of MSHS was tested in a quiescent droplet and monitored with bright-field microscopy (Figure 4c). Under an external magnetic field, the movement of MSHS with a velocity of ~20 μm/s was observed. When the magnetic field direction changed, MSHS immediately followed the direction with a reduced velocity of ~12 μm/s. Thus, the precise control of the magnetic field gradient can efficiently manipulate the navigation of MSHS, driving them to reach and accumulate at the target region. However, a negligible migration was observed for individual Fe_3O_4 nanoparticles due to hydrodynamic and colloidal interactions.[26] Given a hydrodynamic diameter and velocity of ~700 nm and 20 μm/s, respectively, the force generated by MSHS on the order of 3 pN was sufficient to efficiently manipulate MSHS across most of the viscoelastic mediums, thus rendering MSHS

DOI: 10.1021/jacs.5b12149
J. Am. Chem. Soc. 2016, 138, 2090−2093

to be a powerful platform for the magnetic control/manipulation of transport processes.

In summary, submicron hierarchically structured MSHS have successfully been synthesized via the combination of a top-down microfluidics approach along with a bottom-up approach exploiting controlled phase separation and self-assembly. Central to this approach is the use of PEG and MNPs for the generation of double emulsion and single-hole assembly. Besides remarkable monodispersity and tunable magnetic properties, the resulting MSHS fully capitalize on both the multifunctional properties of MNPs and container features of the single-hole hollow spheres. Thus, they can potentially serve as a smart platform. The MSHS could load payloads in a selective way with different size because the diameter of the hole is tunable (smart loading); transport the payloads in a precise route with controllable speed under an external static magnetic field (smart transport); and release the payloads as manipulated when a high-frequency magnetic field was applied as a remote-controlled stimuli (smart release). More interestingly, the entire process can be visualized under the guard assisted by magnetic imaging. We envision this discovery of the hierarchically structured MSHS may lead to further development of new concepts and architectures of nanocontainers, thus allowing for more opportunities in biomedicine and other fields.

■ ASSOCIATED CONTENT

Supporting Information

The Supporting Information is available free of charge on the ACS Publications website at DOI: 10.1021/jacs.5b12149.

Experimental details and additional data (PDF)

■ AUTHOR INFORMATION

Corresponding Authors

*yaoli@iccas.ac.cn

*gaomy@iccas.ac.cn

Notes

The authors declare no competing financial interest.

■ ACKNOWLEDGMENTS

This work was supported by the Chinese Academy of Sciences (YZ201424), the National Natural Science Foundation of China (2014M561073, 21573250), and the Program for Young Outstanding Scientists of ICCAS (Y41Z011). We thank Prof. Yilin Wang for helpful discussions.

■ REFERENCES

(1) Chen, M.; Ye, C.; Zhou, S.; Wu, L. *Adv. Mater.* **2013**, *25*, 5343.

(2) (a) Im, S. H.; Jeong, U.; Xia, Y. N. *Nat. Mater.* **2005**, *4*, 671. (b) Guan, G. J.; Zhang, Z. P.; Wang, Z. Y.; Liu, B. H.; Gao, D. M.; Xie, C. G. *Adv. Mater.* **2007**, *19*, 2370. (c) Hyun, D. C.; Lu, P.; Choi, S.-I.; Jeong, U.; Xia, Y. *Angew. Chem., Int. Ed.* **2013**, *52*, 10468. (d) Liu, D. Y.; Peng, X. X.; Wu, B. H.; Zheng, X. Y.; Chuong, T. T.; Li, J. L.; Sun, S. G.; Stucky, G. D. *J. Am. Chem. Soc.* **2015**, *137*, 9772.

(3) (a) Li, X. M.; Zhou, L.; Wei, Y.; El-Toni, A. M.; Zhang, F.; Zhao, D. Y. *J. Am. Chem. Soc.* **2015**, *137*, 5903. (b) Wang, W.; Zhang, M. J.; Xie, R.; Ju, X. J.; Yang, C.; Mou, C. L.; Weitz, D. A.; Chu, L. Y. *Angew. Chem., Int. Ed.* **2013**, *52*, 8084.

(4) Lim, Y. T.; Kim, J. K.; Noh, Y. W.; Cho, M. Y.; Chung, B. H. *Small* **2009**, *5*, 324.

(5) (a) Gao, J.; Gu, H.; Xu, B. *Acc. Chem. Res.* **2009**, *42*, 1097. (b) Lin, B.; Su, H.; Jin, R.; Li, D.; Wu, C.; Jiang, X.; Xia, C.; Gong, Q.; Song, B.; Ai, H. *Sci. Bull.* **2015**, *60*, 1272.

(6) Lewandowski, W.; Fruhnert, M.; Mieczkowski, J.; Rockstuhl, C.; Górecka, E. *Nat. Commun.* **2015**, *6*, 6590.

(7) Singh, G.; Chan, H.; Baskin, A.; Gelman, E.; Repnin, N.; Král, P.; Klajn, R. *Science* **2014**, *345*, 1149.

(8) Corr, S. A.; Byrne, S. J.; Tekoriute, R.; Meledandri, C. J.; Brougham, D. F.; Lynch, M.; Kerskens, C.; O'Dwyer, L.; Gun'ko, Y. K. *J. Am. Chem. Soc.* **2008**, *130*, 4214.

(9) Qiu, P. H.; Jensen, C.; Charity, N.; Towner, R.; Mao, C. B. *J. Am. Chem. Soc.* **2010**, *132*, 17724.

(10) Park, J. H.; von Maltzahn, G.; Zhang, L.; Schwartz, M. P.; Ruoslahti, E.; Bhatia, S. N.; Sailor, M. J. *Adv. Mater.* **2008**, *20*, 1630.

(11) Yu, X.; Zhu, J. T. *J. Controlled Release* **2011**, *152*, e128.

(12) Zarzar, L. D.; Sresht, V.; Sletten, E. M.; Kalow, J. A.; Blankschtein, D.; Swager, T. M. *Nature* **2015**, *518*, 520.

(13) Utada, A. S.; Lorenceau, E.; Link, D. R.; Kaplan, P. D.; Stone, H. A.; Weitz, D. A. *Science* **2005**, *308*, 537.

(14) Liu, S. Q.; Deng, R. H.; Li, W. K.; Zhu, J. T. *Adv. Funct. Mater.* **2012**, *22*, 1692.

(15) Ku, K. H.; Shin, J. M.; Kim, M. P.; Lee, C. H.; Seo, M. K.; Yi, G. R.; Jang, S. G.; Kim, B. J. *J. Am. Chem. Soc.* **2014**, *136*, 9982.

(16) Xia, Y.; Nguyen, T. D.; Yang, M.; Lee, B.; Santos, A.; Podsiadlo, P.; Tang, Z.; Glotzer, S. C.; Kotov, N. A. *Nat. Nanotechnol.* **2011**, *6*, 580.

(17) Cheng, W.; Tang, K.; Qi, Y.; Sheng, J.; Liu, Z. *J. Mater. Chem.* **2010**, *20*, 1799.

(18) Jun, Y. W.; Seo, J. W.; Cheon, J. *Acc. Chem. Res.* **2008**, *41*, 179.

(19) Yao, L.; Xu, S. *Angew. Chem., Int. Ed.* **2009**, *48*, 5679.

(20) Park, J.; An, K.; Hwang, Y.; Park, J. G.; Noh, H. J.; Kim, J. Y.; Park, J. H.; Hwang, N. M.; Hyeon, T. *Nat. Mater.* **2004**, *3*, 891.

(21) Laurent, S.; Forge, D.; Port, M.; Roch, A.; Robic, C.; Vander Elst, L.; Muller, R. N. *Chem. Rev.* **2008**, *108*, 2064.

(22) Hickey, R. J.; Haynes, A. S.; Kikkawa, J. M.; Park, S. J. *J. Am. Chem. Soc.* **2011**, *133*, 1517.

(23) Gizzatov, A.; Key, J.; Aryal, S.; Ananta, J.; Cervadoro, A.; Palange, A. L.; Fasano, M.; Stigliano, C.; Zhong, M.; Di Mascolo, D.; Guven, A.; Chiavazzo, E.; Asinari, P.; Liu, X.; Ferrari, M.; Wilson, L. J.; Decuzzi, P. *Adv. Funct. Mater.* **2014**, *24*, 4584.

(24) Hyun, D. C.; Lu, P.; Choi, S. I.; Jeong, U.; Xia, Y. *Angew. Chem., Int. Ed.* **2013**, *52*, 10468.

(25) Thomas, C. R.; ferris, D. P.; Lee, J. H.; Choi, E.; Cho, M. H.; Kim, E. S.; Stoddart, F.; Shin, J. S.; Cheon, J.; Zink, J. I. *J. Am. Chem. Soc.* **2010**, *132*, 10623.

(26) Chen, O.; Riedemann, L.; Etoc, F.; Herrmann, H.; Coppey, M.; Barch, M.; Farrar, C. T.; Zhao, J.; Bruns, O. T.; Wei, H.; Guo, P.; Cui, J.; Jensen, R.; Chen, Y.; Harris, D. K.; Cordero, J. M.; Wang, Z. W.; Jasanoff, A.; Fukumura, D.; Reimer, R.; Dahan, M.; Jain, R. K.; Bawendi, M. G. *Nat. Commun.* **2014**, *5*, 5093.

DOI: 10.1021/jacs.5b12149
J. Am. Chem. Soc. 2016, 138, 2090−2093